Analytical Methods

ROYAL SOCIETY OF CHEMISTRY

PAPER

View Article Online
View Journal | View Issue

Cite this: *Anal. Methods*, 2021, **13**, 337

ZnO/SiO_2 core/shell nanowires for capturing CpG rich single-stranded DNAs†

Marina Musa, [a] Takao Yasui, *[abc] Kazuki Nagashima, [bd] Masafumi Horiuchi,[a] Zetao Zhu,[a] Quanli Liu,[a] Taisuke Shimada, [a] Akihide Arima, [a] Takeshi Yanagida [de] and Yoshinobu Baba*[acf]

Received 19th November 2020
Accepted 18th December 2020

DOI: 10.1039/d0ay02138e

rsc.li/methods

Atomic layer deposition (ALD) is capable of providing an ultrathin layer on high-aspect ratio structures with good conformality and tunable film properties. In this research, we modified the surface of ZnO nanowires through ALD for the fabrication of a ZnO/SiO_2 (core/shell) nanowire microfluidic device which we utilized for the capture of CpG-rich single-stranded DNAs (ssDNA). Structural changes of the nanowires while varying the number of ALD cycles were evaluated by statistical analysis and their relationship with the capture efficiency was investigated. We hypothesized that finding the optimum number of ALD cycles would be crucial to ensure adequate coating for successful tuning to the desired surface properties, besides promoting a sufficient trapping region with optimal spacing size for capturing the ssDNAs as the biomolecules traverse through the dispersed nanowires. Using the optimal condition, we achieved high capture efficiency of ssDNAs (86.7%) which showed good potential to be further extended for the analysis of CpG sites in cancer-related genes. This finding is beneficial to the future design of core/shell nanowires for capturing ssDNAs in biomedical applications.

Introduction

Extraordinary properties of nanostructured materials have led to their evolution as zero-dimensional nanoparticles,[1,2] one-dimensional nanotubes and nanowires,[3,4] two-dimensional nanosheets[5] and nanoplates,[6] and three-dimensional nanoballs[7] and nanoflowers.[8] Among these nanomaterials, nanowires have shown good potential in various applications due to their exceptionally high surface-to-volume ratio and strong structure.[9,10] Owing to these advantages, their applications have been broadened to include the recognition of biomolecules[11–15] and aptamer-incorporated nanowires based on single-stranded DNAs (ssDNAs) or RNA oligonucleotides have received considerable interest in biosensing,[16–18] disease diagnoses[19,20] and drug deliveries.[21–23] Among the materials studied, ZnO nanowires grown by a hydrothermal method have been widely used due to their several advantages which include low fabrication cost, low temperature-driven growth, high fabrication yield[24] and feasibility for tuning structural properties of the nanowires; hence ZnO nanowires have the promise of applications in diverse fields.[25–27] However, some researchers reported a toxicity risk when using ZnO based materials;[28–31] and hence, surface coating on ZnO nanowires, especially by the widely used silicon dioxide (SiO_2),[32,33] has become a countermeasure to prevent dissolution of Zn^{2+}. SiO_2 based materials have been widely used in solid-phase extraction of nucleic acids,[34,35] a common method for the adsorption, purification and isolation of nucleic acids which relies on a reversible interaction between the nucleic acids and the solid support. Hence we chose to fabricate ZnO/SiO_2 (core/shell) nanowires for capturing ssDNAs.

For fabrication of the ZnO/SiO_2 (core/shell) nanowires, ZnO nanowires were grown through a hydrothermal method followed by surface modification through atomic layer deposition (ALD). ALD is a robust vapor phase method based on sequential, self-limiting reactions enabling the formation of ultrathin layer films with precise thickness and good uniformity.[36] Although ALD is a powerful technique for achieving coating thicknesses at the nanometer level, it is crucial to ensure conformal coating of the whole nanowire framework as the conformal coating determines the success of tuning to the desired surface

[a]*Department of Biomolecular Engineering, Graduate School of Engineering, Nagoya University, Furo-cho, Chikusa-ku, Nagoya 464-8603, Japan. E-mail: yasui@chembio.nagoya-u.ac.jp; babaymtt@chembio.nagoya-u.ac.jp; Tel: +81-52-789-4611; +81-52-789-4664*

[b]*Japan Science and Technology Agency (JST), Precursory Research for Embryonic Science and Technology (PRESTO), 4-1-8 Honcho, Kawaguchi, Saitama 332-0012, Japan*

[c]*Institute of Nano-Life-Systems, Institutes of Innovation for Future Society, Nagoya University, Furo-cho, Chikusa-ku, Nagoya 464-8603, Japan*

[d]*Department of Applied Chemistry, Graduate School of Engineering, The University of Tokyo, 7-3-1 Hongo, Bunkyo-ku, Tokyo 113-8656, Japan*

[e]*Institute for Materials Chemistry and Engineering, Kyushu University, 6-1 Kasuga-Koen, Kasuga, Fukuoka 816-8580, Japan*

[f]*Institute of Quantum Life Science, National Institutes for Quantum and Radiological Science and Technology, Anagawa 4-9-1, Inage-ku, Chiba 263-8555, Japan*

† Electronic supplementary information (ESI) available. See DOI: 10.1039/d0ay02138e

properties.[37,38] We furthered our investigation by varying the number of ALD cycles to 10, 25, 55, 100 and 200 cycles which is expected to cause remarkable changes to the structure of the nanowire framework due to the increase in coating thickness, and finally, to influence the capture efficiency of ssDNAs.

The ZnO/SiO_2 nanowires were embedded in a microchip device that was integrated with a syringe pump system and applied for capturing CpG rich ssDNAs. The uncaptured ssDNAs were collected in a centrifugation tube and then quantified using qPCR. ssDNAs with the CpG rich sequence have become a binding material of interest especially for aptamers which can be further extended as capture probes for the recognition of DNA methylation on CpG sites, a widely known biomarker in cancer-related genes.[39,40] As capturing occurs while the ssDNAs traverse through the nanowire arrays under an applied flow rate, there should be a suitable nanowire spacing in the trapping region to capture them. Although the dispersedly distributed nanowires are foreseen as a good platform for the trapping region, we supposed that for capturing small biomolecules such as ssDNAs, there should be an optimum spacing between the nanowires to achieve maximum capture efficiency.

Methodology

PDMS microchannel mold fabrication

The mold for fabricating a polydimethylsiloxane (PDMS) microchannel was formed on a 3-inch N-type <100> silicon wafer (Advantech Co., Ltd., Japan). The silicon wafer was spin-coated with 3 mL SU-8 3005 (Nippon Kayaku., Ltd., Japan), baked at 95 °C for 3 min and then subjected to photolithography with UV energy of 200 mJ cm^{-2} for two microchannel patterns formation on one silicon wafer. This was followed by post-baking at 65 °C and 95 °C for 1 min and 2 min, respectively. Next, the patterns were developed using SU-8 developer (Nippon Kayaku Co., Inc.), rinsed with isopropyl alcohol (IPA) (Kanto Chemical Co., Inc., Japan) and by silanization treatment with trichloro(1*H*,1*H*,2*H*,2*H*-perfluorooctyl)silane (Merck KGaA, Germany) for 2 h. The resulting silicon wafer which had two photolithographed-SU-8 microchannel patterns with dimensions of 10 mm length, 5 mm width and 10 μm height was later used as a mold for the PDMS microchannel. A mixture of Silpot184 (Dow Corning Toray Co., Ltd.) and curing agent Catalyst Silpot184 (Dow Corning Toray Co., Ltd.) at a ratio of 10 : 1 was poured into the mold, a vacuum pressure was applied to remove air bubbles and the mold was heated at 80 °C for 2 h. After peeling off the PDMS microchannel, the inlet and outlet holes were then made using a 0.5 mm hole puncher (Harris Uni-Core, USA).

Zinc oxide nanowire microfluidic device fabrication

Fig. 1a illustrates the steps (i) to (x) for the nanowire microfluidic device fabrication process. A pre-cleaned fused silica substrate with 20 mm × 20 mm × 0.5 mm dimensions (Crystal Base Co., Ltd., Japan) (step i of Fig. 1a) was spin-coated with

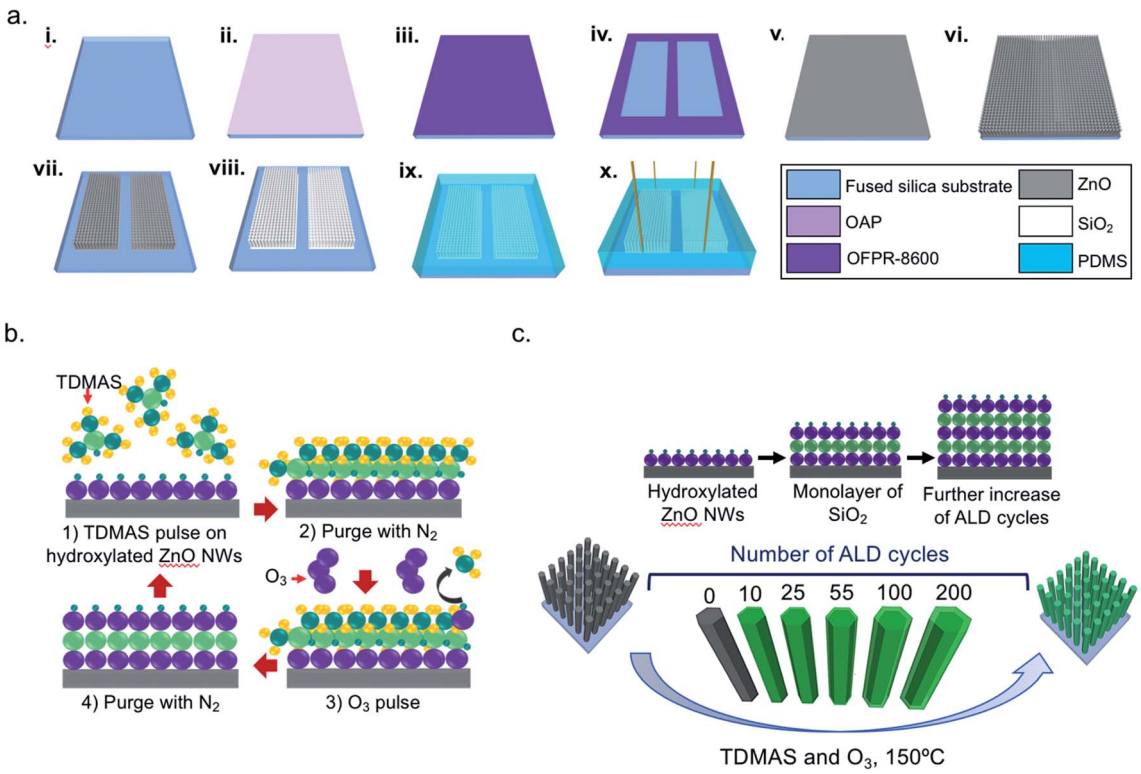

Fig. 1 Schematic illustrations of the ZnO/SiO_2 nanowire microfluidic device fabrication process. (a) Steps (i) to (x) in the microfluidic device fabrication. (b) Details of ALD (step viii) using tris(dimethylamino)silane (TDMAS) and ozone (O_3). (c) Surface modification done to obtain different layer thicknesses by varying the number of ALD cycles as 10, 25, 55, 100 and 200 cycles.

1,1,1,3,3,3-hexamethyldisilazane (OAP, Tokyo Ohka Kogyo Co., Ltd., Japan) and then with OFPR8600 (Tokyo Ohka Kogyo Co., Ltd.) (steps ii and iii, respectively). Next (step iv), photolithography was performed to make two areas for the nanowire growth which each had a length of 10 mm and width of 5 mm. The pattern areas were developed using NMD-3 solution (Tokyo Ohka Kogyo Co., Ltd.). An RF-sputtering machine (SVC-700RF I, Sanyu Electron Co., Ltd., Japan) was utilized to sputter a seed layer of ZnO (thickness, 130 nm) on the substrate for 10 min (step v). Hydrothermal growth of ZnO nanowires was performed by immersing the substrate into a mixture of 40 mM hexamethylenetetramine (HMTA, Wako Pure Chemical Industries, Ltd., Japan) and 40 mM zinc nitrate hexahydrate (Thermo Fisher Scientific Inc.) followed by heating at 95 °C for 3 h (step vi). The OFPR8600 was then removed using acetone (Kanto Chemical Co., Inc.) leaving the nanowires on the desired areas (step vii).

After fabrication of ZnO nanowires, an ALD system (Savannah G2, Ultratech Inc., USA) was used to deposit a thin layer of SiO_2 to fabricate core/shell nanowires (Fig. 1a, step viii). The conditions used were: precursors, tris(dimethylamino) silane (TDMAS) and ozone; temperature, 150 °C; number of ALD cycles, 10, 25, 55, 100 and 200. The resulting fused silica substrate with nanowires was then attached with the PDMS microchannel (step ix). The surfaces of the PDMS and the nanowire-grown substrate were first treated using a plasma etching apparatus (Meiwafosis Co., Ltd., Japan) and then heated at 180 °C for 2 min to assist the bonding process. A 0.5 mm diameter polyetheretherketone (PEEK) tube (Institute of Microchemical Technology Co., Ltd., Japan) was then inserted into the inlet hole and into the outlet hole (Fig. 1a, step x).

FESEM and STEM-EDS characterization of nanowires

A field emission scanning electron microscope (FESEM) (SUPRA 40VP Carl Zeiss, Germany) was utilized to characterize the surface morphology of the nanowires. Elemental mappings of the ZnO/SiO_2 core/shell nanowires were obtained using a scanning transmission electron microscope (JSM-7610F, JEOL, Japan) equipped with an energy dispersive X-ray spectrometer (STEM-EDS) operated at an acceleration voltage of 30 kV. The images were obtained with 512 × 384 pixels at a scan rate of 0.1 ms and they were integrated for 100 cycles. The peaks of Zn Kα (8.630 keV), O Kα (0.525 keV), and Si Kα (1.739 keV) were used to construct the images (ESI Fig. 1†). The statistical analysis of the coating thickness, diameter, length, aspect ratio and spacing between nanowires was performed with an image processing program, Image J using the images from FESEM and STEM-EDS. Because of the dispersed distribution of nanowires, spacings between them were measured at a low height (evaluation at 700 nm from the nanowire bottom) and at an upper region (evaluation at 700 nm from the nanowire top).

Zeta potential measurement

The zeta potential of 50 ng μL^{-1} DNA in Millipore water solution was measured at 25 °C using a dynamic-light scattering spectrophotometer (ZETASIZER Nano-ZS Malvern Panalytical, UK). ZnO/SiO_2 nanowires were fabricated on a glass substrate (26 mm wide × 37 mm long × 1.0 mm thickness) followed by zeta potential measurement (ELSZ-2000, Otsuka Electronics, Japan) in Millipore water at 25 °C.

Capture experiment of ssDNA using the nanowire microfluidic device

The ssDNAs, primers and probes used in this experiment were obtained from Invitrogen, Themo Fisher Scientific, Inc.; their sequences were: (i) ssDNA, 5′-ATACGCGTACTGCGGTCGC-GATCGCGCTCTCGCGCTGACGGTGCGTCGCGCGTACGCGATT-3′; (ii) forward primer, 5′-ACGCGTACTGCGGTCG-3′; (iii) reverse primer, 5′-GCGTACGCGCGACG-3′; and (iv) probe, 5′-FAM-ATCGCGCTCTCGCGCTGACGG-3′. 50 ng μL^{-1} of DNA was prepared by dissolving the stock DNA in Millipore water. The capture experiment was performed using a syringe pump system (KDS-200, KD Scientific Inc., USA) at a flow rate of 5 μL min^{-1}. 50 μL of Millipore water was introduced prior to sample introduction to remove any possible contaminates. Then, 50 μL of 50 ng μL^{-1} DNA was introduced into the inlet of the microfluidic device and the recovered amount was collected in a 1 mL centrifuge tube.

Quantifications of DNA

The recovered ssDNAs were analyzed using a PIKOREAL 96 real-time polymerase chain reaction (RT-PCR) system (Thermo Fisher Scientific Inc.). A mixture containing 1 μL DNA solution, 3.5 μL Millipore water, 5 μL TaqMan® Gene Expression Master Mix (Applied Biosystems, Thermo Fisher Scientific Inc., USA) and 0.5 μL of the Custom TaqMan® Gene Expression Assays (Applied Biosystems, Thermo Fisher Scientific Inc.) was pipetted into a 96-well reaction plate, sealed with an optical seal (Applied Biosystems, Thermo Fisher Scientific) and RT-PCR was run. The protocol for RT-PCR was carried out using the cycling conditions 2 min at 50 °C, 10 min at 95 °C, 50 cycles of 15 s at 95 °C and 1 min at 60 °C. The amount of captured DNA was calculated by deducting the amount of recovery from the input DNA.

Results and discussion

Surface modification using ALD

Surface modification of the nanowire through ALD for the fabrication of core/shell nanowires has been proven able to improve surface adsorption of target molecules.[41–43] In the present research, we grew ZnO nanowires by a hydrothermal method followed by surface modification using ALD to fabricate the ZnO/SiO_2 (core/shell) nanowires. Fig. 1b schematically showed details for fabrication of the core/shell nanowires using ALD. The reactant and co-reactant used were tris(dimethylamino)silane (TDMAS) and ozone (O_3), respectively. The process was initiated with the exposure of the first reactant to hydroxylated ZnO nanowires followed by nitrogen (N_2) purging to remove the unreacted chemical species. The next reaction involved the introduction of co-reactant as the oxygen source followed by N_2 purging which resulted in monolayer formation.

The sequence was repeated for the following numbers of ALD cycles: 10, 25, 55, 100 and 200 to yield nanowires with different coating thicknesses (Fig. 1c). The sequential deposition of the reactant and co-reactant led to the ultrathin film with good conformality.

Characterizations and statistical analysis of ZnO/SiO_2 while varying number of ALD cycles

STEM-EDS was utilized to obtain a more detailed analysis for the composition of ZnO/SiO_2 nanowires. Successful formation of a very thin SiO_2 film can be observed starting from 10 cycles followed by increment in film thickness as the number of ALD cycles further increased until 200 cycles were reached (Fig. 2a and ESI figure†). The resulting SiO_2 thickness had a linear relationship with the number of ALD cycles with an approximate growth rate of 0.13 nm per cycle (Fig. 2b). Surface morphology of the nanowires was characterized using FESEM which indicated an increase in the size of nanowires with increasing number of ALD cycles (Fig. 2c).

The dependence of nanowire structural properties on number of ALD cycles was investigated by statistical analysis of important parameters which include the diameter, length, aspect ratio and spacing between nanowires. Fig. 3a summarizes the size distribution of bare ZnO nanowires and the maximum peak was for the diameter range of 60–90 nm and for the length range of 1.6–1.8 μm. A consistent increase in the diameter and length of the nanowires could be observed with increasing number of ALD cycles suggesting uniform deposition of SiO_2 film was provided by ALD (Fig. 3b). Aspect ratios, in the range of 15 to 19, were decreasing as the number of ALD cycles increased in Fig. 3c. Due to the dispersed distribution of the nanowires (Fig. 2c), statistical analysis of available spacing between nanowires was done randomly at lower and upper regions. A decreasing trend in spacing between nanowires was observed as ALD cycle numbers increased for spacing in the range of 15.9 nm to 34.9 nm and 43.5 nm to 60.9 nm, at the lower and upper regions, respectively (Fig. 3d). Increasing the number of ALD cycles resulted in the increase in nanowire diameter with a drop in aspect ratio, and eventually reduced the spacing volume between the nanowires.

Influence of SiO_2 coating thickness on the capture efficiency of ssDNAs

Since finding the optimum number of ALD cycles is crucial to ensure conformal coating of film layer on the whole nanowire framework, we further investigated the impact of the number of

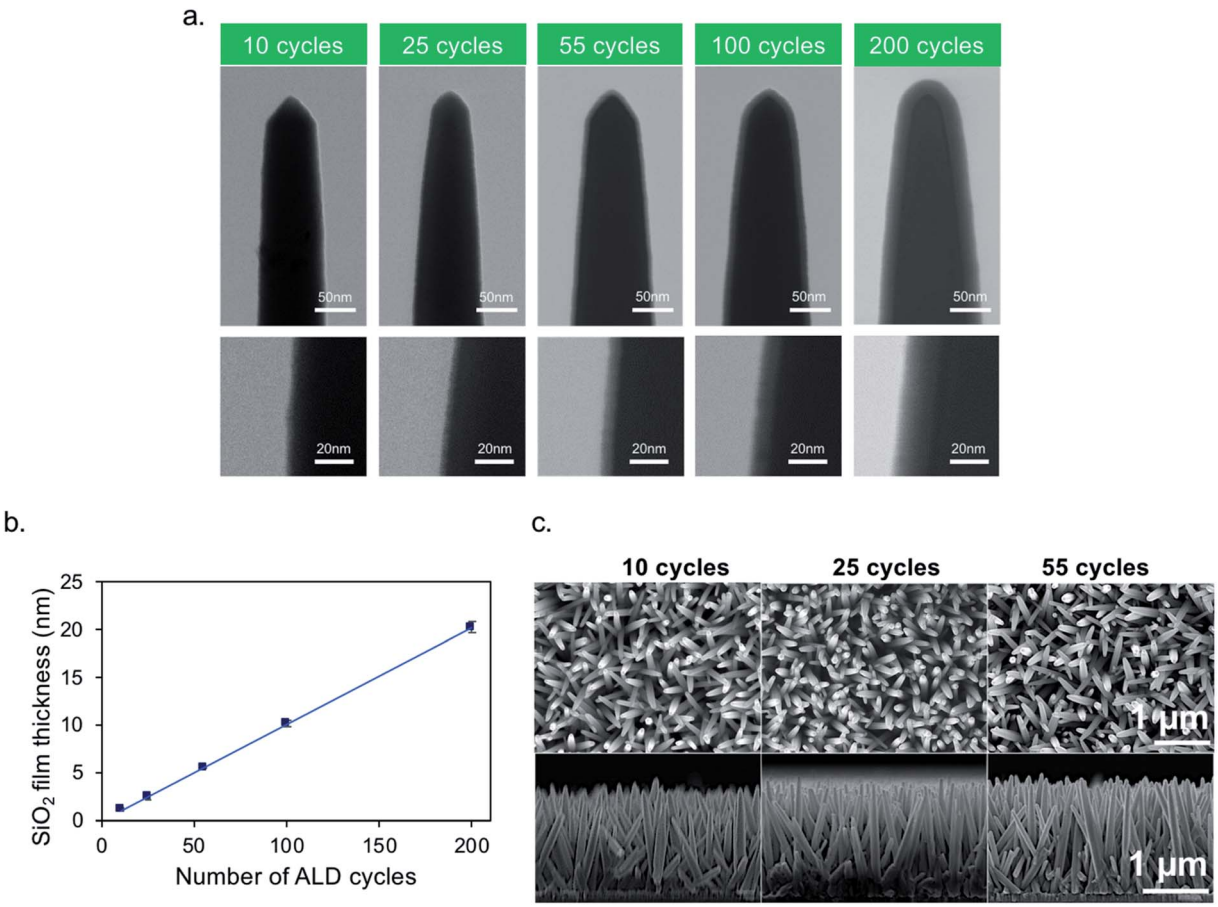

Fig. 2 Characterizations of metal oxide nanowires. (a) STEM micrographs of ZnO/SiO_2 nanowires fabricated with varying number of ALD cycles: 10, 25, 55, 100 and 200 cycles. (b) Plot of the SiO_2 thickness as a function number of ALD cycles. (c) FESEM images of ZnO/SiO_2 nanowires fabricated with 10 cycles, 25 cycles and 55 ALD cycles: (upper row) top and (lower) cross-sectional views.

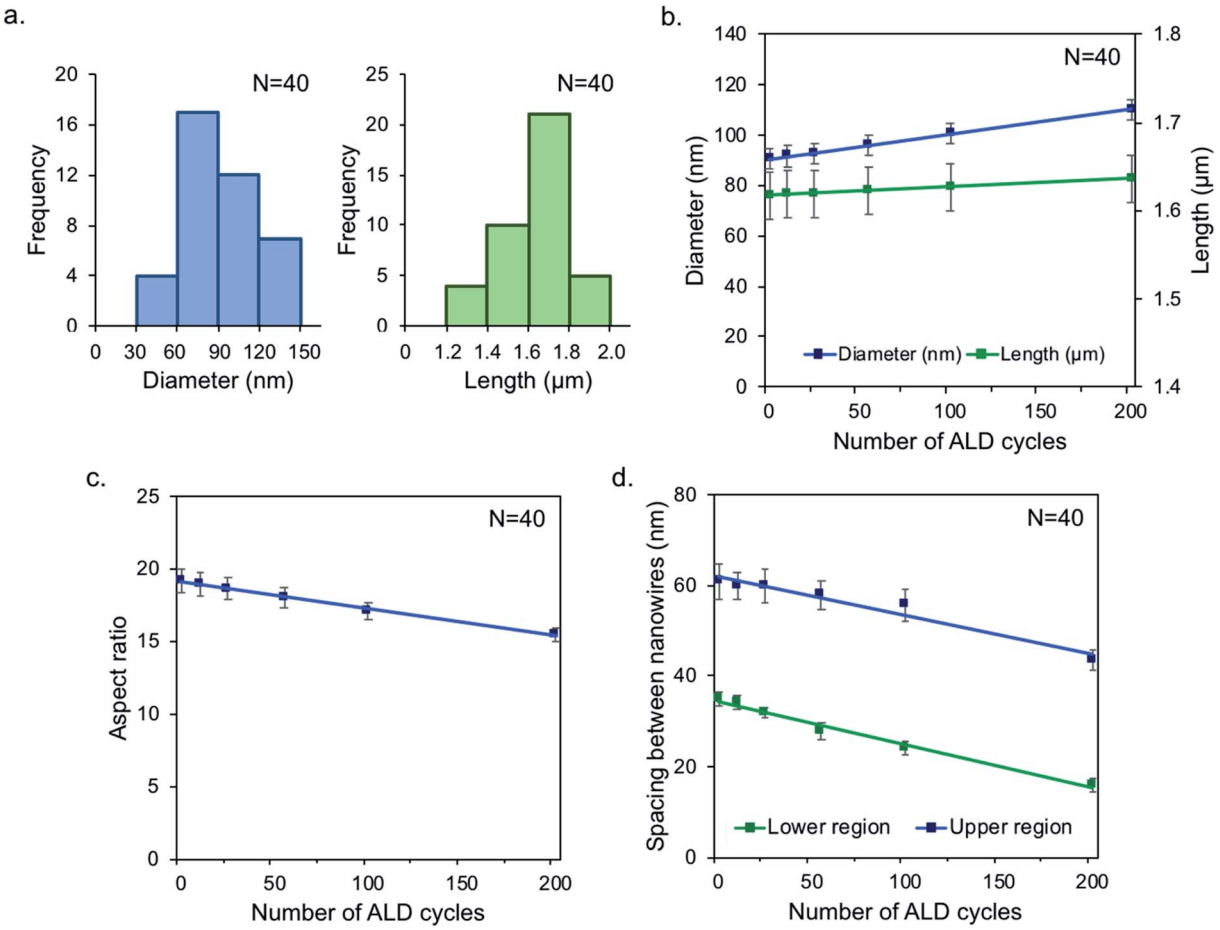

Fig. 3 Statistical analysis of fabricated nanowires. (a) Size distribution of bare ZnO nanowires. (b) Diameter and length. (c) Aspect ratio. (d) Spacing between nanowires.

ALD cycles on the capture efficiency of ssDNAs. We observed that ZnO/SiO_2 (core/shell) nanowires fabricated by 10 ALD cycles showed slight improvement of the capture efficiency (Fig. 4a and ESI Fig. 2†). The increasing trend of the capture efficiency could be observed from 0 to 55 cycles followed by a declining trend until 200 cycles. The zeta potential of ZnO/SiO_2 nanowires while changing the number of ALD cycles was measured in neutral pH to investigate the net surface charges which might be correlated to the changes in capture efficiency (Fig. 4b). Negative zeta potential values indicate the presence of SiO_2 layers which are negatively charged in neutral pH. The high zeta potential value exhibited at 10 cycles (−16.19 mV) was possibly due to a thin SiO_2 layer coating that led to interference of charges from the core ZnO nanowires. A consistent trend in zeta potential values, from −24.7 mV to −26.0 mV was observed for nanowires fabricated by 25 ALD cycles to 200 cycles (Fig. 3b) leading to remarkable changes in the capture efficiency (Fig. 3a). Therefore, we concluded the sufficient coating is crucial to ensure the tuning of surface properties to the desired materials.

Further increases in the ALD cycle numbers will cause structural changes to the nanowires and eventually reduce the spacing between the nanowires. Although a higher number of ALD cycles resulted in a bigger nanowire size (Fig. 3b), however, we observed a decline in the capture efficiency from 55 cycles (Fig. 4a) onwards possibly due to a more significant decrease in aspect ratio at 100 and 200 cycles (Fig. 3c), hence the interaction areas, which are the surface of nanowires available for capturing the ssDNAs, were limited. Besides, the low aspect ratio is correlated with the increase in the diameter of nanowires resulting in smaller spacing between nanowires. Considering that the gyration radius of the ssDNA is $R_g < 10$ nm, there should be suitable spacing between the nanowires as interactions are more likely to occur among the nanowires on the periphery of the array as the ssDNAs traverse through the framework. We supposed that the capture efficiency of the ssDNAs was governed by the spacing between nanowires (Fig. 3d) which decreased with increasing ALD cycle numbers.

Here, we proposed a model for capturing ssDNAs based on the structural effect while varying ALD cycle numbers (Fig. 4c). Apart from the interactions between SiO_2 and the nucleobase side,[44] interactions are possible with the phosphate side based on the theory of hard and soft acids and bases although the surface of ssDNA and SiO_2 are negatively charged. This is corresponding with previous method, which reported on the DNA adsorption on several metal oxide nanoparticles with negative

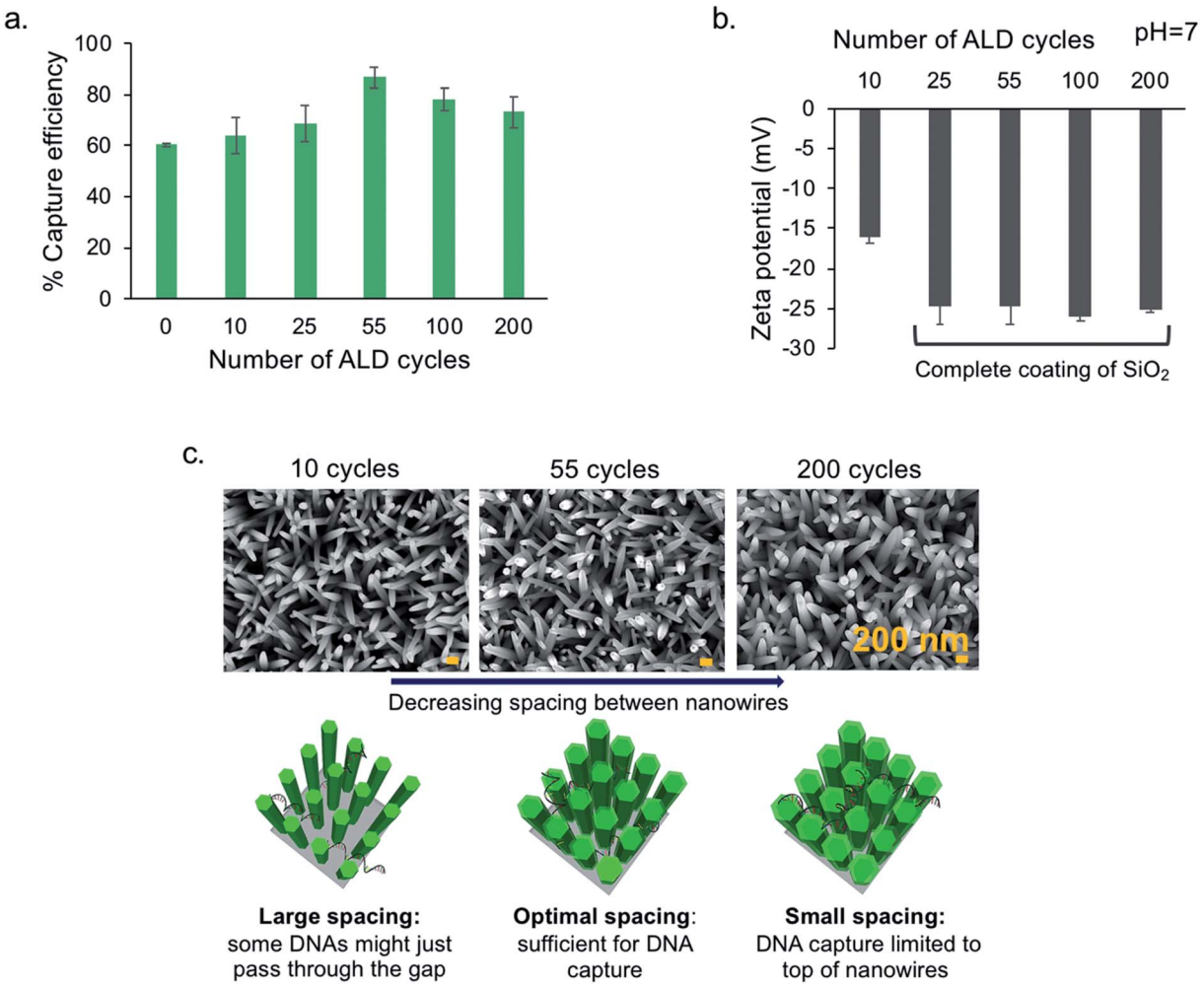

Fig. 4 Influence of numbers of ALD cycles on DNA capture efficiency. (a) Capture efficiency of ssDNAs on ZnO/SiO_2 nanowires fabricated for different numbers of ALD cycles. Experimental conditions: 50 μL of 50 ng μL^{-1} DNA solution; flow rate 5 μL min^{-1}. (b) Zeta potential of ZnO/SiO_2 nanowires fabricated for different numbers of ALD cycles at pH = 7. Error bars show the standard error for a series of measurements ($N = 3$). (c) Proposed model explaining the effect of structural changes on DNA capture.

charged surface.[45,46] Low capture efficiency at 10 cycles (64.3%) and 25 cycles (69.0%) was possibly due to an unsatisfactory trapping region allowing some of the ssDNAs to traverse through the nanowires without being captured. The highest capture efficiency was achieved at 55 cycles (86.7%) due to the sufficient optimal spacing as a sieving region. Further increase in ALD cycle number from 100 cycles (78.3%) to 200 cycles (73.2%) resulted in a decline in the capture efficiency due to small spacing for capturing ssDNAs, hence the capture might be inhibited and occurring only at the top of the nanowires. We hypothesized that the design of the nanowire framework with an optimum trapping region will promote capturing as the ssDNAs traverse through the nanowire arrays, hence ensuring high capture efficiency.

Conclusion

In this research, we proved surface modification by coating a thin SiO_2 layer on ZnO nanowires using ALD was able to enhance the capture efficiency of ssDNAs. In order to obtain the maximum capture efficiency, finding the optimum number of ALD cycles is crucial to ensure adequate coating of the whole nanowire framework with the desired materials and to provide a suitable trapping region to capture the ssDNAs. We proposed that in the design of the framework, an optimum spacing between nanowires is crucial to ensure a suitable trapping region as the ssDNAs traverse through the nanowires. Besides, by using the optimum condition, higher capture efficiency (86.7%) was achieved compared to our previously reported study (60%).[47] This research provides fundamental findings based on the design of the core/shell nanowire framework in microfluidic devices which will be useful in future development of applications for high capture efficiency of ssDNAs.

Author contributions

M. M., T. Yasui, N. K., T. Yanagida and Y. B. planned and designed the experiment. M. M. and N. K. performed the

experiments. M. M., T. Yasui, N. K., M. H., Z. Z., Q. L., T. S., A. A. analyzed data. M. M. and T. Yasui wrote the paper.

Conflicts of interest

There are no conflicts to declare.

Acknowledgements

This research was supported by PRESTO (JPMJPR19H9), Japan Science and Technology Agency (JST), the JSPS Grant-in-Aid for Scientific Research (S) 18H05243, the JSPS Grant-in-Aid for Scientific Research (B) 18H02009, the JSPS Grant-in-Aid for Exploratory Research 20K21124, the JSPS Grant-in-Aid for Scientific Research on Innovative Areas "Chemistry for Multimolecular Crowding Biosystems", and research grants from each of the following: the Murata Science Foundation, Advanced Technology Institute Research Grants 2019, Foundation of Public Interest of Tatematsu, the Nitto Foundation, the G-7 Scholarship Foundation, the Nanotechnology Platform Program (Molecule and Material Synthesis) of the Ministry of Education, Culture, Sports, Science and Technology (MEXT), and the Cooperative Research Program of the "Network Joint Research Center for Materials and Devices".

References

1 J. N. Tiwari, R. N. Tiwari and K. S. Kim, *Prog. Mater. Sci.*, 2012, **57**, 724–803.
2 P. K. Mishra, H. Mishra, A. Ekielski, S. Talegaonkar and B. Vaidya, *Drug Discovery Today*, 2017, **22**, 1825–1834.
3 C. Zhang, Y. Yan, Y. S. Zhao and J. Yao, *Annu. Rep. Prog. Chem., Sect. C: Phys. Chem.*, 2013, **109**, 211–239.
4 R. C. Arbulu, Y. Jiang, E. J. Peterson and Y. Qin, *Angew. Chem., Int. Ed.*, 2018, **57**, 5813–5817.
5 M. Wang, X. Liu, P. Song, X. Wang, F. Xu and X. Zhang, *Int. J. Biol. Macromol.*, 2019, **128**, 621–628.
6 S. Shi, X. Chen, J. Wei, Y. Huang, J. Weng and N. Zheng, *Nanoscale*, 2016, **8**, 5706–5713.
7 M. Guo, J. Balamurugan, X. Li, N. H. Kim and J. H. Lee, *Small*, 2017, **13**, 1701275.
8 W. Lei, D. Liu, J. Zhang, P. Zhu, Q. Cui and G. Zou, *Cryst. Growth Des.*, 2009, **9**, 1489–1493.
9 S. Rahong, T. Yasui, T. Yanagida, K. Nagashima, M. Kanai, A. Klamchuen, G. Meng, Y. He, F. Zhuge, N. Kaji, T. Kawai and Y. Baba, *Sci. Rep.*, 2014, **4**, 5252.
10 T. Yasui, S. Rahong, K. Motoyama, T. Yanagida, Q. Wu, N. Kaji, M. Kanai, K. Doi, K. Nagashima, M. Tokeshi, M. Taniguchi, S. Kawano, T. Kawai and Y. Baba, *ACS Nano*, 2013, **7**, 3029–3035.
11 T. Shimada, T. Yasui, A. Yokoyama, T. Goda, M. Hara, T. Yanagida, N. Kaji, M. Kanai, K. Nagashima, Y. Miyahara, T. Kawai and Y. Baba, *Lab Chip*, 2018, **18**, 3225–3229.
12 Z. Lin, Y. Li, J. Gu, H. Wang, Z. Zhu, X. Hong, Z. Zhang, Q. Lu, J. Qiu, X. Wang, J. Bao and T. Wu, *Adv. Funct. Mater.*, 2018, **28**, 1802482.
13 M. Nuzaihan, U. Hashim, M. K. M. Arshad, S. R. Kasjoo, S. F. A. Rahman, A. R. Ruslinda, M. F. M. Fathil, R. Adzhri and M. M. Shahimin, *Biosens. Bioelectron.*, 2016, **83**, 106–114.
14 T. Adam and U. Hashim, *Biosens. Bioelectron.*, 2015, **67**, 656–661.
15 J. Wang and N. Hui, *Sens. Actuators, B*, 2019, **281**, 478–485.
16 M. Liu, Q. Yin, Y. Chang, Q. Zhang, J. D. Brennan and Y. Li, *Angew. Chem., Int. Ed.*, 2019, **58**, 8013–8017.
17 H. M. Meng, H. Liu, H. Kuai, R. Peng, L. Mo and X. B. Zhang, *Chem. Soc. Rev.*, 2016, **45**, 2583–2602.
18 J. Kong, J. Zhu, K. Chen and U. F. Keyser, *Adv. Funct. Mater.*, 2019, **29**, 1807555.
19 M. Liu, X. Yu, Z. Chen, T. Yang, D. Yang, Q. Liu, K. Du, B. Li, Z. Wang, S. Li, Y. Deng and N. He, *J. Nanobiotechnol.*, 2017, **15**, 1–16.
20 X. Meng, Z. Liu, Y. Cao, W. Dai, K. Zhang, H. Dong, X. Feng and X. Zhang, *Adv. Funct. Mater.*, 2017, **27**, 1605592.
21 O. Boyacioglu, C. H. Stuart, G. Kulik and W. H. Gmeiner, *Mol. Ther.–Nucleic Acids*, 2013, **2**, e107.
22 Y. Wan, L. Wang, C. Zhu, Q. Zheng, G. Wang, J. Tong, Y. Fang, Y. Xia, G. Cheng, X. He and S. Y. Zheng, *Cancer Res.*, 2018, **78**, 798–808.
23 M. Mie, R. Matsumoto, Y. Mashimo, A. E. G. Cass and E. Kobatake, *Mol. Biol. Rep.*, 2019, **46**, 261–269.
24 N. A. Alshehri, A. R. Lewis, C. Pleydell-Pearce and T. G. G. Maffeis, *J. Saudi Chem. Soc.*, 2018, **22**, 538–545.
25 Q. Liu, T. Yasui, K. Nagashima, T. Yanagida, M. Hara, M. Horiuchi, Z. Zhu, H. Takahashi, T. Shimada, A. Arima and Y. Baba, *J. Phys. Chem. C*, 2020, **124**, 20563–20568.
26 X. Zhao, K. Nagashima, G. Zhang, T. Hosomi, H. Yoshida, Y. Akihiro, M. Kanai, W. Mizukami, Z. Zhu, T. Takahashi, M. Suzuki, B. Samransuksamer, G. Meng, T. Yasui, Y. Aoki, Y. Baba and T. Yanagida, *Nano Lett.*, 2019, **20**, 599–605.
27 Q. Liu, T. Yasui, K. Nagashima, T. Yanagida, M. Horiuchi, Z. Zhu, H. Takahashi, T. Shimada, A. Arima and Y. Baba, *Anal. Sci.*, 2020, **36**, 1125–1129.
28 R. S. Alghsham, S. R. Satpathy, S. R. Bodduluri, B. Hegde, V. R. Jala, W. Twal, J. A. Burlison, M. Sunkara and B. Haribabu, *Front. Immunol.*, 2019, **10**, 2604.
29 K. H. Müller, J. Kulkarni, M. Motskin, A. Goode, P. Winship, J. N. Skepper, M. P. Ryan and A. E. Porter, *ACS Nano*, 2010, **4**, 6767–6779.
30 S. L. Chia and D. T. Leong, *Heliyon*, 2016, **2**, e00177.
31 M. Ramasamy, M. Das, S. S. A. An and D. K. Yi, *Int. J. Nanomed.*, 2014, **9**, 3707.
32 M. Afsal, C. Y. Wang, L. W. Chu, H. Ouyang and L. J. Chen, *J. Mater. Chem.*, 2012, **22**, 8420–8425.
33 H. W. Kim, H. S. Kim, H. G. Na and J. C. Yang, *Vacuum*, 2012, **86**, 789–793.
34 G. R. M. Duarte, C. W. Price, J. L. Littlewood, D. M. Haverstick, J. P. Ferrance, E. Carrilho and J. P. Landers, *Analyst*, 2010, **135**, 531–537.
35 P. E. Vandeventer, J. S. Lin, T. J. Zwang, A. Nadim, M. S. Johal and A. Niemz, *J. Phys. Chem. B*, 2012, **116**, 5661–5670.
36 R. W. Johnson, A. Hultqvist and S. F. Bent, *Mater. Today*, 2014, **17**, 236–246.

37 J.-H. Kim, A. Katoch and S. S. Kim, *Sens. Actuators, B*, 2016, **222**, 249–256.
38 T. G. Ulusoy, A. Ghobadi and A. K. Okyay, *J. Mater. Chem. A*, 2014, **2**, 16867–16876.
39 D. R. Masser, D. R. Stanford, N. Hadad, C. B. Giles, J. D. Wren, W. E. Sonntag, A. Richardson and W. M. Freeman, *Age*, 2016, **38**, 1–14.
40 S. Catuogno, C. L. Esposito and V. De Franciscis, *Pharmaceuticals*, 2016, **9**, 69.
41 T. Shimada, T. Yasui, A. Yonese, T. Yanagida, N. Kaji, M. Kanai, K. Nagashima, T. Kawai and Y. Baba, *Micromachines*, 2020, **11**, 610.
42 T. Yasui, T. Yanagida, S. Ito, Y. Konakade, D. Takeshita, T. Naganawa, K. Nagashima, T. Shimada, N. Kaji, Y. Nakamura, I. A. Thiodorus, Y. He, S. Rahong, M. Kanai, H. Yukawa, T. Ochiya, T. Kawai and Y. Baba, *Sci. Adv.*, 2017, **3**, e1701133.
43 C. Guan, X. Wang, Q. Zhang, Z. Fan, H. Zhang and H. J. Fan, *Nano Lett.*, 2014, **14**, 4852–4858.
44 B. Shi, Y. K. Shin, A. A. Hassanali and S. J. Singer, *J. Phys. Chem. B*, 2015, **119**, 11030–11040.
45 B. Liu, L. Ma, Z. Huang, H. Hu, P. Wu and J. Liu, *Mater. Horiz.*, 2018, **5**, 65–69.
46 R. Pautler, E. Y. Kelly, P. J. J. Huang, J. Cao, B. Liu and J. Liu, *ACS Appl. Mater. Interfaces*, 2013, **5**, 6820–6825.
47 H. Takahashi, T. Yasui, K. Shinjo, N. Kaji, A. Okamoto and Y. Baba, *22nd International Conference on Miniaturized Systems for Chemistry and Life Sciences*, MicroTAS 2018, Chemical and Biological Microsystems Society, 2018, pp. 1886–1888.

